



HAL
open science

Epitaxial growth of the candidate ferroelectric Rashba material SrBiO₃ by pulsed laser deposition

Gaetan Verdierre, N Gauquelin, D Jannis, Y. A Birkhölzer, S Mallik, J Verbeeck, M. Bibes, G Koster

► **To cite this version:**

Gaetan Verdierre, N Gauquelin, D Jannis, Y. A Birkhölzer, S Mallik, et al.. Epitaxial growth of the candidate ferroelectric Rashba material SrBiO₃ by pulsed laser deposition. *APL Materials*, 2023, 11, 10.1063/5.0138222 . hal-04288423

HAL Id: hal-04288423

<https://hal.science/hal-04288423>

Submitted on 16 Nov 2023

HAL is a multi-disciplinary open access archive for the deposit and dissemination of scientific research documents, whether they are published or not. The documents may come from teaching and research institutions in France or abroad, or from public or private research centers.

L'archive ouverte pluridisciplinaire **HAL**, est destinée au dépôt et à la diffusion de documents scientifiques de niveau recherche, publiés ou non, émanant des établissements d'enseignement et de recherche français ou étrangers, des laboratoires publics ou privés.

Epitaxial growth of the candidate ferroelectric Rashba material SrBiO₃ by pulsed laser deposition

Cite as: APL Mater. 11, 031109 (2023); <https://doi.org/10.1063/5.0138222>

Submitted: 09 December 2022 • Accepted: 28 February 2023 • Published Online: 17 March 2023

 G. Verdierre,  N. Gauquelin,  D. Jannis, et al.



View Online



Export Citation



CrossMark



APL Materials







Special Topic: Materials Challenges for Nonvolatile Memory

[Read Now!](#)

Epitaxial growth of the candidate ferroelectric Rashba material SrBiO₃ by pulsed laser deposition

Cite as: APL Mater. 11, 031109 (2023); doi: 10.1063/5.0138222
Submitted: 9 December 2022 • Accepted: 28 February 2023 •
Published Online: 17 March 2023



G. Verdierre,^{1,2}  N. Gauquelin,³  D. Jannis,³  Y. A. Birkhölzer,¹  S. Mallik,² J. Verbeeck,³ M. Bibes,^{2,a)} 
and G. Koster¹ 

AFFILIATIONS

¹MESA+ Institute for Nanotechnology, University of Twente, Enschede, The Netherlands

²Unité Mixte de Physique CNRS/Thales, Palaiseau, France

³Electron Microscopy for Materials Research (EMAT), University of Antwerp, Antwerp, Belgium

^{a)}Author to whom correspondence should be addressed: manuel.bibes@cnsr-thales.fr

ABSTRACT

Among oxides, bismuthates have been gaining much interest due to their unique features. In addition to their superconducting properties, they show potential for applications as topological insulators and as possible spin-to-charge converters. After being first investigated in their bulk form in the 1980s, bismuthates have been successfully grown as thin films. However, most efforts have focused on BaBiO₃, with SrBiO₃ receiving only little attention. Here, we report the growth of epitaxial films of SrBiO₃ on both TiO₂-terminated SrTiO₃ and NdO-terminated NdScO₃ substrates by pulsed laser deposition. SrBiO₃ has a pseudocubic lattice constant of ~4.25 Å and grows relaxed on NdScO₃. Counter-intuitively, it grows with a slight tensile strain on SrTiO₃ despite a large lattice mismatch, which should induce compressive strain. High-resolution transmission electron microscopy reveals that this occurs as a consequence of structural domain matching, with blocks of 10 SrBiO₃ unit planes matching blocks of 11 SrTiO₃ unit planes. This work provides a framework for the synthesis of high quality perovskite bismuthates films and for the understanding of their interface interactions with homostructural substrates.

© 2023 Author(s). All article content, except where otherwise noted, is licensed under a Creative Commons Attribution (CC BY) license (<http://creativecommons.org/licenses/by/4.0/>). <https://doi.org/10.1063/5.0138222>

I. INTRODUCTION

Since the early 1980s, most electronic devices have relied on the use of complementary metal-oxide semiconductor (CMOS) transistors. However, it has been recently suggested that more energy-efficient transistors could be designed based on a ferromagnetic material whose magnetization would be switched by a multiferroic through magnetoelectric coupling and read by a spin-orbit material through spin-charge conversion.¹ An alternative to this so-called MESO (magnetoelectric spin-orbit) device, which would not require magnetization switching, relies on controlling the spin-to-charge conversion by the inverse Rashba-Edelstein effect present in a ferroelectric material. Such a control has been recently demonstrated at low temperature using oxide-based two-dimensional electron gases² and at room temperature with a ferroelectric Rashba semiconductor (FERSC)³, GeTe.⁴

In this context, FERSCs are emerging as a very promising family of materials for future spin-based low-power applications. However, these materials are very scarce, and the sole confirmed candidate so far is GeTe. If their bandgap is small as in GeTe, FERSCs tend to show leakage when subjected to an electric field applied to switch their polarization. This is motivating the search for FERSCs in other materials families and, in particular, within perovskite oxides.^{2,5,6} For instance, it has been recently proposed that when strained, perovskite SrBiO₃ (SBO) would be a FERSC.⁷ This is due to a large spin-orbit coupling (SOC) induced by Bi *d*-orbitals concomitant with the existence of a strain-induced phase transition to a ferroelectric phase. Sufficiently strained SBO would then be a FERSC with an electrically switchable Rashba coefficient of $\alpha_R = 1.68 \text{ eV \AA}$ (much higher than in perovskite oxide 2DEGs⁸⁻¹⁰). In addition, SBO has been suggested as a possible candidate building block in perovskite heterostructures in which spatially separated

two-dimensional hole and electron gases would appear,¹¹ further motivating its exploration in the thin film form.

SBO crystallizes in the monoclinic system, with the space group $P2_1/n$ ($a = 5.948 \text{ \AA}$, $b = 6.0951 \text{ \AA}$, $c = 8.4854 \text{ \AA}$, and $\beta = 90.063^\circ$). Its pseudocubic lattice parameter is $a_c \approx 4.25 \text{ \AA}$. The related compound BaBiO_3 (BBO) was extensively studied in the 1970s as a type II superconductor with critical temperature $T_c = 30 \text{ K}$ ¹² when hole doped, which prompted interest in other members of the bismuthate family. SBO and related compounds were investigated in the late 1990s for properties similar to those observed in doped BBO.¹³ K-doped SBO is a type II superconductor with $T_c = 12 \text{ K}$.¹⁴ Undoped BBO has recently regained interest as a potential topological insulator^{15–17} and as a buffer layer for the growth of oxides with a large lattice constant.¹⁸ Epitaxial growth of BBO thin films by molecular beam epitaxy and pulsed laser deposition (PLD)^{18–20} was reported. However, very few growth studies concerning SBO were published. Here, we report the growth of epitaxial SBO by PLD and the first attempts to induce a high level of compressive strain in an epitaxial bismuthate thin film.

II. EXPERIMENTAL

SBO thin films were grown on TiO_2 -terminated SrTiO_3 (001) (STO) and NdScO_3 (110) (NSO) substrates using pulsed laser deposition (PLD) and characterized by *in situ* reflection high-energy electron diffraction (RHEED) and x-ray photoelectron spectroscopy (XPS) with a monochromatized $\text{Al K}\alpha$ (1486.6 eV) x-ray source. Additional *ex situ* characterization was performed with an x-ray diffraction (XRD) setup. STO substrates were prepared by a wet etching step in a buffered hydrogen fluoride (BHF) solution, followed by a 1.5 h annealing step at 950°C in a tube furnace with a flow of pure oxygen gas.²¹ NSO substrates were prepared by a 4 hours annealing step at 1000°C , also in a flow of oxygen, followed by two subsequent etching steps in buffered HF and sodium hydroxide.²² A stoichiometric target of Sr–Bi–O (Toshiba, purity 99.99%) was used for the PLD growth with a KrF laser (Coherent, 25 ns) at a fluence of 1.9 J/cm^2 and a spot size of 0.589 mm^2 . The substrate temperature was kept at 525°C , and the O_2 background pressure was set to 10^{-2} mbar. The distance between the target and the substrate was kept constant at 50 mm. A repetition rate of 1 Hz and a total of 1500 pulses were used for the 70 nm thick SBO layers for growth on STO. 200 pulses were used when definitive growth parameters for SBO were established as it yielded thick enough films for the purpose of studying strain relaxation. The samples were post-annealed

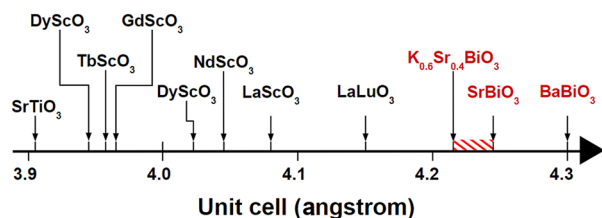


FIG. 1. Schematic of the unit cells of different perovskites of interest to study SrBiO_3 . The hatched area corresponds to $\text{K}_x\text{Sr}_{1-x}\text{BiO}_3$ for x in $[0, 0.6]$. Potential substrates are labeled in black, and parent compounds of interest are in red.

in situ at the growth temperature under an O_2 background pressure of 100 mbar, slowly cooled down to 300°C , kept at this temperature for 20 min to maximize the oxygen loading in the crystal, and finally cooled down to room temperature. Lattice parameters of different substrates and of SBO and its parent compounds are given in Fig. 1.

III. RESULTS

The growth of SBO was first optimized by depositing thick and relaxed (75–100 nm) SBO thin films on STO. The film growth was monitored by *in situ* RHEED, and the structure of the films was studied using x-ray diffraction. We investigated the influence of the growth temperature, the growth oxygen pressure, the laser spot size, the post-anneal procedure, and the presence of a capping layer. *In situ* RHEED measurements, which are represented in Fig. 2, indicate a two-dimensional growth with a flat, long-range ordered surface. From these data, we can deduce an in plane lattice parameter of 4.3 \AA for SBO, which is slightly bigger than the bulk value, but consistent with XRD measurements performed on the films presented in this study (see later). In order to perform *ex situ* measurements, we found that a capping layer was required as SBO appeared to quickly degrade when directly exposed to air. We investigated two capping layers: amorphous aluminum oxide and ultra-thin STO. The growth of a single layer of STO as a cap yielded higher quality films. We then established a phase diagram as a function of temperature and pressure for the growth of SBO on STO [Fig. 3(a)]. Changing the pressure and temperature influences the nature of the crystal grown, with two predominant crystal structures depending on the sticking of bismuth; see Fig. 3(b). If the bismuth does not stick, the main phase grown is (111)-oriented rock salt strontium oxide with a lattice parameter of $\sim 3.65 \text{ \AA}$.²³ If the bismuth does stick, the main phase grown is a (001)-oriented

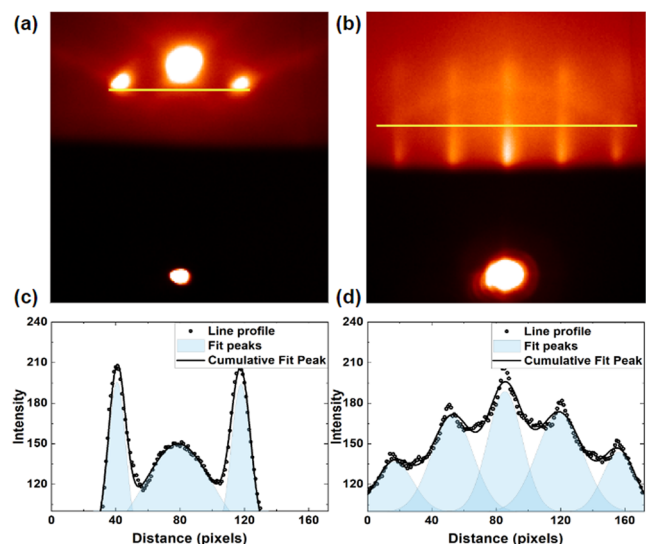


FIG. 2. RHEED signal acquired (a) on the substrate before starting the growth and (b) after cooling the sample down. The plot profile of the intensity along the yellow lines are presented in (c) and (d) for STO and SBO, respectively.

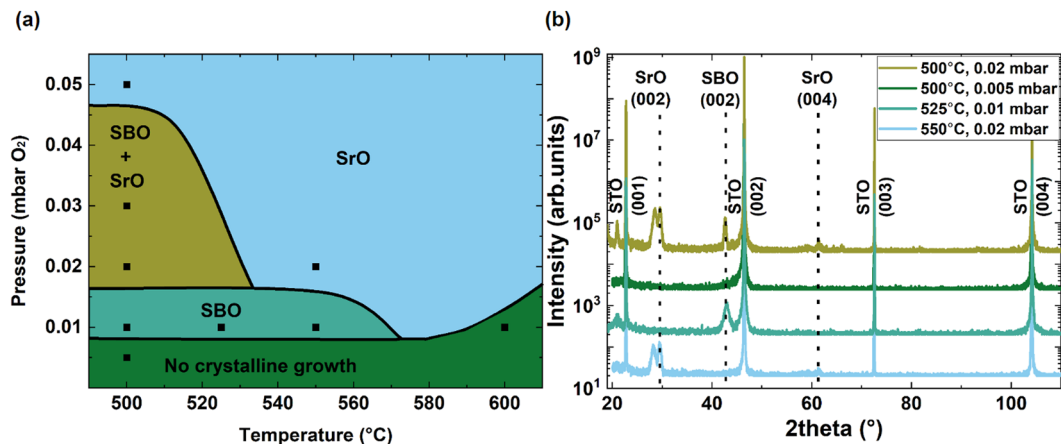


FIG. 3. (a) SBO phase diagram established for the growth of SBO. (b) XRD spectra acquired in different zones shown in (a). It is worth noting that the oxygen growth pressure is the most critical parameter to optimize when trying to grow bismuthates.

perovskite with an ~ 4.25 Å lattice parameter, corresponding to pure SBO. As visible from Fig. 3(a), the oxygen pressure window in which single-phase SBO can be grown is relatively narrow. Therefore, the oxygen partial pressure is the most critical parameter to optimize when trying to reproduce these growth experiments.

The chemical composition and electronic structure of the films were studied using *in situ* XPS. Figures 4(a) and 4(b) show the Sr 3*d* and Bi 4*f* core-level spectra for a 75 nm thick SBO film. The data confirm the presence of Sr 2+ and Bi nominally 4+, as expected. After subtraction of a Shirley background, the peaks were fitted with Gaussian–Lorentzian peaks with a 30% Gaussian character. The FWHM of the peaks of a given element was enforced to be the same, and the ratio of the areas was enforced to be 0.75 for the case of Bi 4*f* and 0.66 for the case of Sr 3*d*. In addition, film stoichiometry of the surface can be estimated from the area of the XPS peaks, which results in a Sr:Bi:O ratio of 21:26:52 ± 5%. These values are indicative of stoichiometric SBO within a reasonable margin of uncertainty for XPS quantification attempts based on tabulated relative sensitivity factors and in agreement with the XPS results previously reported on bismuthates.^{18,24}

By using the conditions established above, we attempted to induce epitaxial strain in SBO films by reducing their thickness and growing them on STO and NSO.

The crystal structure of the perovskite SBO thin-films was studied by x-ray diffraction. Figure 5(a) shows the XRD spectra acquired between 15° and 105°, and an inset represents the (002) peak of SBO grown on SrTiO₃ and NdScO₃, respectively. The XRD spectra are characteristic of a (001) oriented single-phase perovskite thin film. From the position of the (002) peak, we infer an out of plane lattice parameter of 4.26 Å for both films, which is in accordance with previous results for SBO films.^{14,25}

The atomic force microscopy (AFM) topography images represented in Figs. 5(a)–5(c) show that the morphology of the surface is greatly affected by the nature of the substrate. SBO grown on NSO is of higher quality, as proven by the presence of atomic steps on the AFM images. We attribute the difference in morphology to the smaller lattice mismatch between the film and the substrate in

the case of NSO. Indeed, the NSO/SBO lattice mismatch is of 4.9%, whereas in the case of STO/SBO, it is more than 8%.

In addition to this difference in morphology, the in-plane lattice parameter of SBO also varies when changing the substrate. From

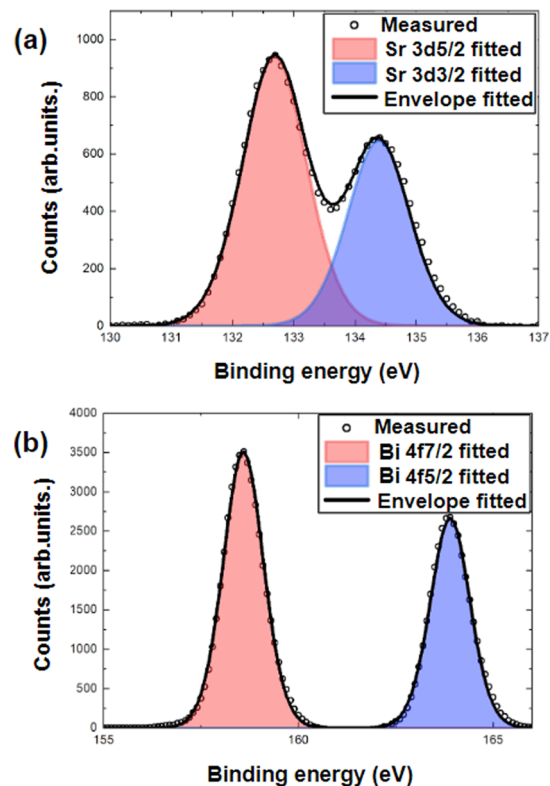


FIG. 4. Surface stoichiometry characterized by XPS: (a) and (b) core-level spectroscopy of Sr 3*d* and Bi 4*f*, respectively.

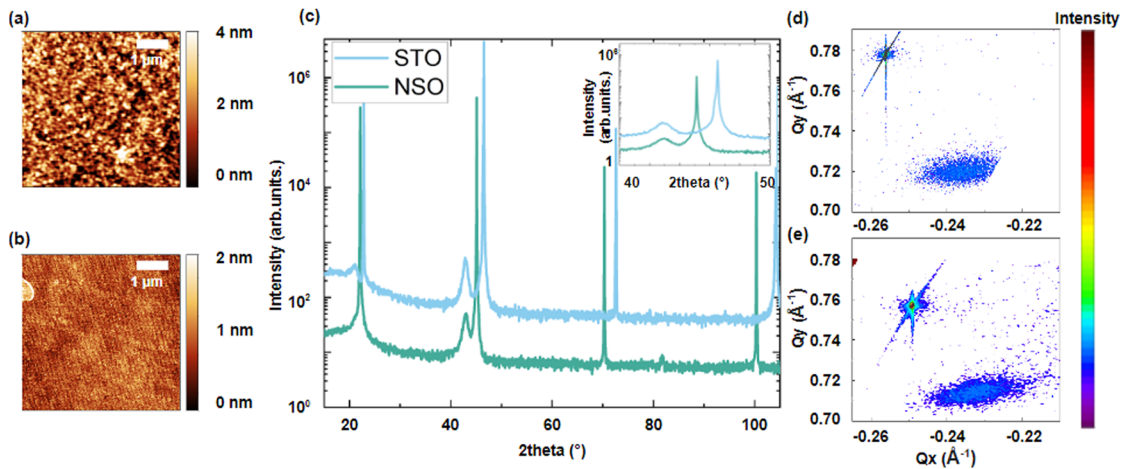


FIG. 5. Effect of the substrate on the growth of SBO thin films: (a) and (b) AFM of the surface of the films grown on STO and NSO, respectively. (c) Symmetric XRD spectra of the films grown on STO and NSO. (d) and (e) Reciprocal space map of the (103) peak of SBO grown on STO and NSO, respectively. The spectra are characteristic of a perovskite single-phase.

TABLE I. Lattice parameters of SrBiO₃ grown on different substrates.

Substrate	Expected compressive strain (%)	SBO \perp lattice parameter (\AA)	SBO \parallel lattice parameter (\AA)	Measured strain
SrTiO ₃	8.8	4.26	4.31	+1.2% (tensile)
NdScO ₃	6.0	4.31	4.31	0% (none)

reciprocal space maps, we observe that SBO grown on STO seems to be subjected to tensile strain, while SBO thin films grown on NSO are relaxed (Table I). This may at first seem counter-intuitive as the lattice constant of SBO is larger than that of STO, but this echoes existing findings for BBO.¹⁸ Indeed, when grown on STO, BBO accommodates the large mismatch with the substrate by naturally forming two buffer layers of rock salt BaO at the interface with the substrate.¹⁸ BBO then grows in such a way that 9 bismuthate u.c. is matching with 10 STO u.c.^{18,20,26} This domain matching causes the bismuthate lattice to quickly relax through the formation of periodic dislocations. In this configuration, BBO grows with a 4.33 \AA lattice parameter. This is slightly smaller than the relaxed lattice parameter of BBO¹² but allows for a 9 to 10 u.c. domain matching. BBO grown on STO thus naturally grows with an almost relaxed lattice parameter even though one could have expected a high level of compressive strain.

In a similar manner, we can infer that in the case of SBO, strain is also regulated by the formation of periodically ordered dislocation sites. However, instead of resulting in a relaxed lattice, it induces tensile strain in the SBO film close to the interface to create matching blocks of multiple unit cells of STO and SBO. From the lattice parameter values deduced from x-ray reciprocal space maps, we expect a dislocation every 9–10 STO u.c., coinciding with 10–11 SBO u.c., which would result in an in-plane lattice parameter of ~ 4.3 \AA for SBO.

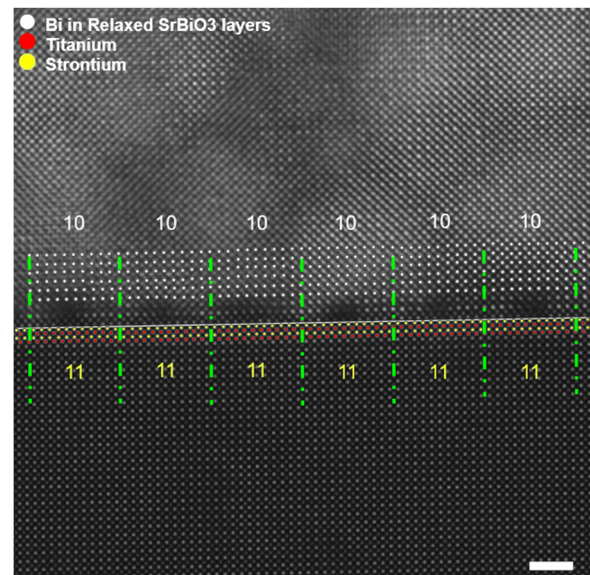


FIG. 6. HAADF imaging of the interface of a thin film of SBO grown on STO. Periodic dislocation sites can be observed at the interface between STO and SBO, every 10 u.c. of SBO, coinciding with 11 STO u.c. The scale bar is 2 nm.

To verify this hypothesis, we imaged the interface of SBO thin films grown on STO by high-angle annular dark field scanning transmission electron microscopy (HAADF-STEM). This analysis is represented in Fig. 6. When examining the interface of SBO thin films grown on STO, we observe indeed the formation of a periodic pattern of 10 u.c. of SBO matching with 11 u.c. of STO. To achieve such a matching pattern, SBO has to expand in-plane and mismatch dislocations have to form periodically. This confirms and explains the tensile nature of the strain induced in SBO layers close to the interface with STO.

The nature of the strain relaxation around the dislocation and how it varies with different substrates will still need to be investigated to determine whether SBO grown by PLD can be ferroelectric. This is subject to further study and beyond the focus of the present article.

IV. CONCLUSION

In conclusion, high-quality SBO films were successfully prepared on TiO₂-terminated STO substrates and MO-terminated rare-earth scandates. The films were found to degrade quickly when exposed to air, but a thin STO or Al oxide capping layer is enough to protect them. Single phase films could only be stabilized in a narrow window of growth pressure and temperature. We clearly observed a strong effect of the lattice mismatch on the crystal quality and the type of growth. Lattice-matched substrates led to a more ordered crystal structure and smoother morphology although the film material in both cases would exhibit strain relaxation. The relaxation occurs via the formation of a very thin interfacial layer, similar to what has been observed in other bismuthates. The successful fabrication of high-quality SBO single-phase films opens the possibility of investigating the strain effects at the interfaces with different substrates and might be suitable for the study of 2D spatially separated hole and electron 2D gases and for spintronic applications using the Edelstein effect.

ACKNOWLEDGMENTS

This work received support from the ERC Advanced grant (Grant No. 833973) “FRESCO” and funding from the European Union’s Horizon 2020 Research and Innovation Program under Grant Agreement No. 823717—ESTEEM3, Van Gogh travel grant, Nuffic, The Netherlands (CF No. 42582SB).

AUTHOR DECLARATIONS

Conflict of Interest

The authors have no conflicts to disclose.

Author Contributions

G. Verdierre: Investigation (lead); Writing – original draft (lead). **N. Gauquelin:** Investigation (supporting). **D. Jannis:** Investigation (equal). **Y. A. Birkhölzer:** Investigation (supporting). **S. Mallik:** Investigation (supporting). **J. Verbeeck:** Investigation (supporting). **M. Bibes:** Conceptualization (equal); Project administration (lead); Writing – review & editing (equal). **G. Koster:** Conceptualization (equal); Writing – review & editing (equal).

DATA AVAILABILITY

The data that support the findings of this study are available from the corresponding author upon reasonable request.

REFERENCES

- ¹S. Manipatruni *et al.*, *Nature* **565**, 35 (2018).
- ²P. Noël *et al.*, *Nature* **580**, 483 (2020).
- ³S. Picozzi, *Front. Condens. Matter Phys.* **2**, 1 (2014).
- ⁴S. Varotto *et al.*, *Nat. Electron.* **4**, 740 (2021).
- ⁵R. Arras *et al.*, *Phys. Rev. B* **100**, 174415 (2019).
- ⁶L. L. Tao and J. Wang, *J. Appl. Phys.* **120**, 234101 (2016).
- ⁷J. Varignon, J. Santamaria, and M. Bibes, *Phys. Rev. Lett.* **122**, 116401 (2019).
- ⁸D. C. Vaz *et al.*, *Phys. Rev. Mater.* **4**, 071001(R) (2020).
- ⁹L. M. Vicente-Arche *et al.*, *Adv. Mater.* **33**, 2102102 (2021).
- ¹⁰S. Varotto *et al.*, *Nature Commun.* **13**, 6165 (2022).
- ¹¹A. Khazraie, I. Elfimov, K. Foyevtsova, and G. A. Sawatzky, *Phys. Rev. B* **101**, 035135 (2020).
- ¹²A. W. Sleight, J. L. Gillson, and P. E. Bierstedt, *Solid State Commun.* **17**, 27 (1975).
- ¹³A. W. Sleight, *Physica C* **514**, 152 (2015).
- ¹⁴S. M. Kazakov *et al.*, *Nature* **390**, 148 (1997).
- ¹⁵G. Trimarchi, X. Zhang, A. J. Freeman, and A. Zunger, *Phys. Rev. B* **90**, 161111 (2014).
- ¹⁶G. Li, B. Yan, R. Thomale, and W. Hanke, *Sci. Rep.* **5**, 10435 (2015).
- ¹⁷B. Khamari, R. Kashikar, and B. R. K. Nanda, *Phys. Rev. B* **97**, 045149 (2018).
- ¹⁸R. L. Bouwmeester *et al.*, *Phys. Status Solidi RRL* **13**, 1800679 (2019).
- ¹⁹G. Kim *et al.*, *Phys. Rev. Lett.* **115**, 057206 (2015).
- ²⁰M. Zapf *et al.*, *Appl. Phys. Lett.* **112**, 141601 (2018).
- ²¹G. Koster, B. L. Kropman, G. J. H. M. Rijnders, D. H. A. Blank, and H. Rogalla, *Appl. Phys. Lett.* **73**, 2920 (1998).
- ²²J. E. Kleibeuker *et al.*, *Adv. Funct. Mater.* **20**, 3490 (2010).
- ²³T. Gagnidze, H. Ma, C. Cancellieri, G.-L. Bona, and F. La Mattina, *Sci. Technol. Adv. Mater.* **20**, 456 (2019).
- ²⁴C. R. Brundle and B. V. Crist, *J. Vac. Sci. Technol. A* **38**, 041001 (2020).
- ²⁵Y. Li *et al.*, *Phys. Rev. Mater.* **3**, 073805 (2019).
- ²⁶L. Jin *et al.*, *Phys. Status Solidi RRL* **14**, 2000054 (2020).